EXPERIMENTAL STUDY OF NANOBUBBLES AND NANODROPLETS ON HYDROPHOBIC/HYDROPHILLIC COMBINED SURFACES

Takahashi K.*[1,2], Nishiyama T. [1,2], Yamada Y. [2] and Takata Y. [2,3]
*Author for correspondence
[1]Department of Aeronautics and Astronautics,
[2]International Institute for Carbon-Neutral Energy Research (WPI-I2CNER),
[3]Department of Mechanical Engineering,
Kyushu University,
Fukuoka, 819-0395,
Japan,
E-mail: takahashi@aero.kyushu-u.ac.jp

ABSTRACT

The effects of surface wettability on nanobubbles and nanodroplets at the solid/liquid and solid/vapor interfaces are studied by using atomic force microscopy (AFM) and environmental scanning electron microscopy (ESEM). Nanobubbles generated by the solvent exchange method appear preferentially on the hydrophobic surface but hydrophilic surface is found to enhance their generation and stability. The interfacial nanobubbles are confirmed to be of spherical-capped shape but the tapping of AFM probe can deform them and the deformed nanobubbles are pretty stable even though two are collapsed into a butterfly shape. Nanodroplets are generated by condensation of water vapor in ESEM. Both the nanodroplets and nanobubbles are of more flattened shape than the macroscopic ones. Micro/nanoscale fabrication techniques of hydrophobic/ hydrophilic combined surface are also discussed.

INTRODUCTION

The initial stage of boiling and condensation is not yet fully understood because the phenomena are in nanometer or molecular scale and there had been no effective experimental tool for it. We could employ only model analysis based on inhomogeneous nucleation theory or molecular dynamics to estimate the phenomena. In these decades, experimental study in heat transfer engineering has reached to tens of micrometer scale using MEMS technique, enabling us to investigate the phase change at the artificial micro cavities, etc. but we are still far from satisfying understanding of the beginning stage of liquid-vapor phase change on solid surfaces. However, recent nanotechnology enables us to investigate the nanoscale targets more easily than ever. For example, AFM has as high spatial resolution as the atoms and is used for measuring not only the topography but many kinds of surface property in sub-nanometer scale. Very tiny gas phase at the liquid/solid interface was first observed by using tapping-mode AFM (TM-AFM) in 2000[1,2] and the Fourier transform infrared spectroscopy successfully confirmed gaseous phase there in 2007[3] but the mechanism of its stability against the huge pressure due to the surface tension is still veiled.

Nanobubbles in bulk liquid or so-called ultrafine bubbles are also attracting interests because of their application for fishery, water purification, and substrate cleaning, and so on. Their stability has been confirmed with the quick-freezing-replica electron microscopy[4] and is supposed due to the electrostatic force of ions or contamination on the liquid/gas interface, both of which reduces the surface tension. On the other hand, interfacial nanobubbles, which exist at the liquid/solid interface, should be strongly affected by the surface property. Several models have been proposed to explain their stability. For example, the gas outflux driven by the Laplace pressure is balanced by gas influx at the contact line, which results in the stabilization of interfacial nanobubbles.[5,6] It is also suggested that the intrinsic nanoscale physical roughness or chemical heterogeneities of the substrates induces the pinning force from contact line and maintain the gas phase there.[7–12] Line tension is another model to explain the flattening of bubble in microscale[13] but its mechanism is still unresolved due to the lack of reliable data of micro/nanoscale bubble. In addition to spherical-capped nanobubbles, micropancakes were observed, of irregular shape with a typical height of 1-2 nm and width of over 1 μm.[14] Nanobubble–micropancake composites were also observed but it is difficult to understand their stability.[15,16]

Water droplet condensation is another topic of long research history and recently attracts increasing interest [17-35], coupled with the microscale wettability control of the heat transfer surface. It is known that dropwise condensation shows one order of magnitude higher performance than the filmwise condensation [36,37]. An experimental study reported that droplets with smaller diameter than 10μm covered only 10% of the surface but achieved at least 50% of the total heat transfer [38], which means we can accomplish several times higher performance of condensation heat transfer if such tiny droplets detach automatically. Recently, by employing micro/nanoscale structure with artificially-controlled wettability was found to remove tiny droplets very efficiently but further understanding of the relationship between surface wettability and droplet structure is highly desired.

In this paper, we summarize our experimental results of nanbubbles and nanodroplets, obtained by using AFM and ESEM, respectively. Highly oriented pyrolytic graphite (HOPG), Teflon amorphous fluoroplastic (AF) thin film, and self-assembled monolayer (SAM) of very high hydrophobicity were used as solid surface with electron or ion beam technique for nanoscale wettability patterning.

EXPERIMENTS OF NANOBUBBLES

Surface Preparation

A highly ordered pyrolytic graphite (HOPG) sample with a thickness of ca. 0.5 mm is peeled from a bulk HOPG (HOPG, SPI-1 Grade, 10×10 mm, Alliance Biosystems Inc., Japan). The surface of this sample has terrace-step structure. The terrace or basal plane is perfectly flat surface due to the carbon atoms arranged in a honeycomb lattice while the step or step edge comes from the breaking of C-C bonds thus shows relatively hydrophilic nature. The roughly measured contact angles of terrace and step are 90° and 75°, respectively.

The sample is fixed on a stainless-steel Petri dish and first immersed in ethanol, which has higher air solubility than water, for several minutes before the ethanol was displaced by pure water prepared by a water purifier (RFP742HA, Advantec, Japan). Both ethanol and water are not degassed. This process creates supersaturated conditions at the HOPG–liquid interface and thereby enhances the formation of nanobubbles of air, which is called as solvent-exchange method. [2,15,39–42] Supersaturation is believed to be an important factor in nanobubble formation. [43,44]

A Teflon AF1600X (DuPont Inc., Wilmington, DE, USA) thin film is another hydrophobic surface for nanobubble experiment, which was formed on a Si substrate from a 0.2-wt% solution of AF1600X with Fluorinert FC-770 (3M Electronics, St. Paul, MN, USA) by the dip-coating method, and it was then baked for 1 hour at 95 °C. Obtained Teflon AF thin film is very thin (50 nm thickness) and very smooth (0.3 nm surface roughness) but its macroscopic contact angle is about 120°. This is one of the highest contact angles for such smooth surface determined only by the material property without the Cassy-Baxter effect of surface roughness. [45,46]

We microscopically modified the wettability of Teflon AF film by using amorphous carbon deposition induced by electron beam, as called electron-beam-induced deposition, which was performed with a Versa 3D Dual Beam scanning electron microscope (FEI company). The deposition region is set in a rectangle shape and deposited amorphous carbon at a dose of 66 nC/μm^2. Obtained macroscopic contact angle of deposited amorphous carbon is 75°, which means the deposited domain is hydrophilic enough compared with the Teflon film, and its height is 3-5nm. We prepared the hydrophilic carbon domains with a width of 300 nm and length of 5 μm in 100-, 400-, and 900-nm intervals as shown later. Nanobubbles are generated by the same solvent exchange method as HOPG sample.

Measurement Methods

Nanobubbles were first observed by TM-AFM[1,2] and remains the most commonly used technique in nanobubble

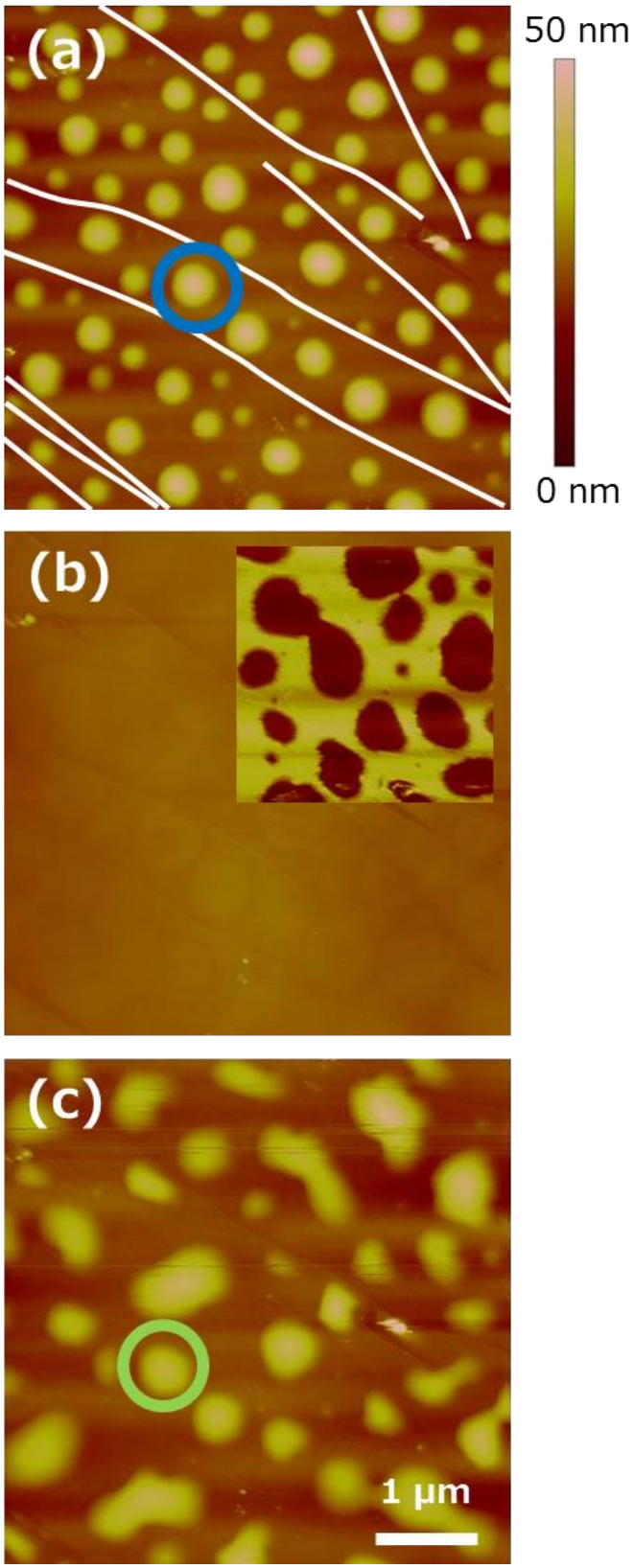

Figure 1 PF-QNM images of nanobubbles at HOPG/water interface measured (a) 45min, (b) 150min, (c) 180min after solvent exchange with a setpoint of 462pN, 2.3nN, 462pN, respectively. DMT model mapping is added in (b)

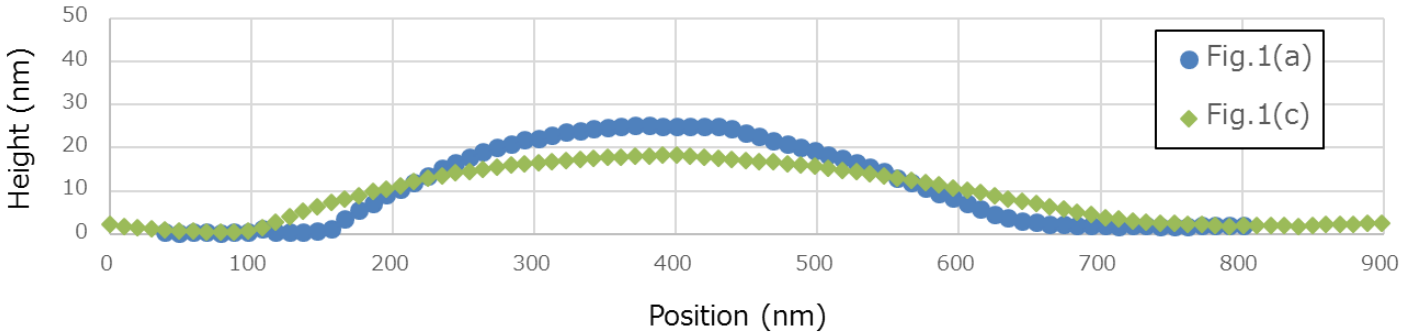

Figure 2 Measured cross sections of interfacial nanobubbles at different peak force setpoints

research.[5,8,47–51] However, because it detects changes in the amplitude of the resonance frequency oscillation of a cantilever, deformation of interfacial nanobubble can be induced by TM-AFM. On the other hand, a recently-developed AFM measurement mode, peak force quantitative nanomechanics (PF-QNM) is advantageous for nanobubble measurement[52–54] because it can control the interactions between the AFM tip and nanobubble by changing the peak force setpoint that determines the strength of the tip approach while TM-AFM keeps the cantilever vibration amplitude constant. We measured the interfacial nanobubbles with a Dimension Icon atomic force microscope (Bruker AXS) and a Scan Asyst Fluid+ cantilever (tip radius 5 nm, spring constant 0.7 N m−1). The liquid temperature was controlled to 25±1.5 °C by using a heater under the petri dish during the AFM measurement.

Results and Discussion

By applying different peak force setpoints from 462 pN to 2.3 nN, AFM images of nanobubbles on HOPG are obtained and listed in Figure 1. The image in Figure 1(a) was obtained 45 min after solvent exchange with the peak force setpoint set at 462 pN, which is a sufficiently weak loading force to measure soft nanobubbles. The white lines there indicate the positions of the steps on the HOPG surface. The interfacial nanobubbles on HOPG appear on the terraced areas and not on the steps mainly due to the wettability difference. The nanobubbles are semispherical with base diameter of 100–500 nm and height of 3–22 nm. The measured contact angle of the nanobubbles is 170° to 174° though the macroscopic contact angle of HOPG surface is about 90°. This tendency is similar to the previous reports, where line tension is introduced to explain the reason of change of the contact angle. A topographical image taken 150 min after solvent exchange applying a setpoint of 2.3 nN is shown in Figure 1(b). Nanobubbles disappeared from the topographical image but they were still detected using the Derjaguin–Muller–Toropov (DMT) model, as inset there. Figure 1(c) is obtained 180 min after solvent exchange with a 462-pN peak force setpoint, again. The coalescence of many nanobubbles was observed and the butterfly-shaped bubbles made from two adjacent spherical bubbles were found stable for more than 50 minutes. We confirmed no nanobubble coalescence occurs at the setpoint of 462 pN, which means nanobubbles in Figure 1(a) are very close to the intrinsic ones without any effect of AFM probe.

We also found that the nanobubbles are flattened by a strong tapping force. Once the position of the contact line of a nanobubble has been moved by the deformation, the nanobubble does not return to its original shape even if the setpoint is decreased to a low load. This is probably due to the pinning effect, which also maintains the butterfly-shaped nanobubbles. The cross sections of an individual nanobubble at the HOPG–water interface indicated by circles in Figures 1(a) and (c) are shown in Figure 2. The shape and contact angle of the nanobubble changed during the PF-QNM measurements and its diameter increased and height decreased, leading to an increase in contact angle from 169° to 174°. Such pinning effect could induce many kinds of irregular shapes of nanobubbles especially when TM-AFM was applied. Our results show that all interfacial nanobubbles without any effect of pressing and tapping of the AFM cantilever are of semisperical shape.

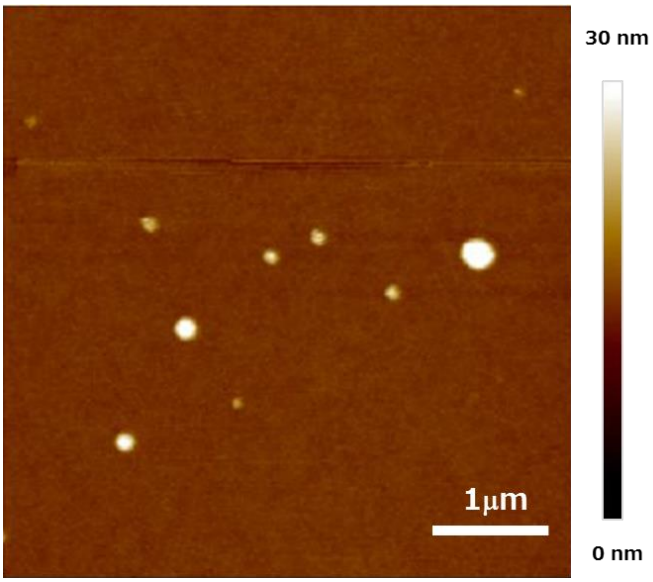

Figure 3 AFM image of nanobubble at Teflon AF/water interface observed two hours after solvent exchange

Figure 3 shows an AFM image of nanobubble at Teflon AF/water interface generated by the same solvent exchange method at almost same temperature as HOPG experiment. Though the contact angle of Teflon AF is much higher than that of HOPG, there was a lower number density of smaller nanobubbles on Teflon AF thin film. Basically the wettability is linked with the interaction between liquid molecules and solid surface and a surface of higher contact angle should be more suitable for bubble generation in the saturated liquid. To understand this contradictory result, we hypothesized that the many hydrophilic steps promote the generation of nanobubbles on the hydrophobic terrace and consequently prepared the Teflon AF surface with hydrophilic amorphous carbon domains of 300nm width as described before. As shown in Figure 4, many interfacial nanobubbles appeared in the vicinity of the hydrophilic domains. This result supports our hypothesis and also nanobubbles shrinkage was not observed in the presence of hydrophilic domains, in contrast to the pure hydrophobic substrate in Figure 3, even 3 days after solvent exchange. Dammer and Lohse reported the gas enrichment at the interface of the liquid and hydrophobic wall, which can stabilize the nanobubbles on hydrophobic surface. When the hydrophilic domain and hydrophobic surface coexist, the gas enrichment on the hydrophobic surface adjacent of the hydrophilic domain can be enhanced by the dissolved air in the vicinity of the hydrophilic domains as an additional source. The promotion of nanobubble generation on the hydrophobic surface near hydrophilic domain can be explained by a similar scenario.

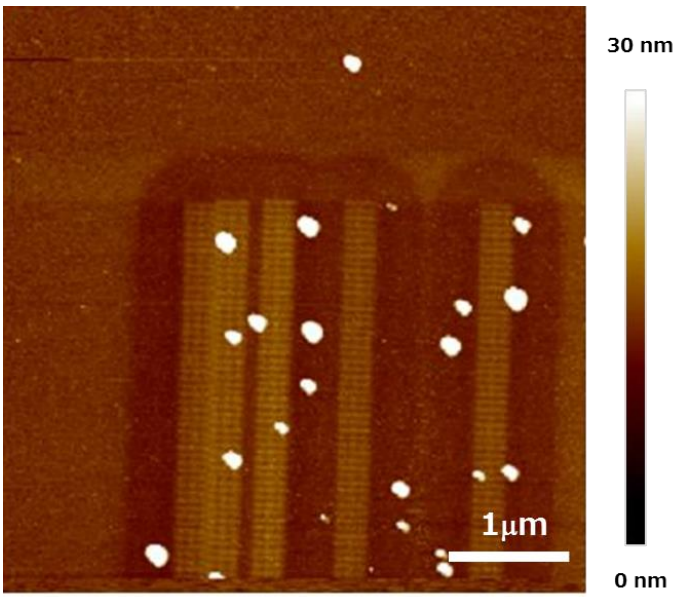

Figure 4 Interfacial nanobubbles observed in the vicinity of the additional hydrophilic domains made of amorphous carbon deposition

EXPERIMENTS OF NANODROPLETS

A silicon substrate with oxidized layer of 2nm thickness were dipped in the 1*H*,1*H*,2*H*,2*H*-perfluoro-*n*-octylphosphonic acid (FOPA; Dojindo Laboratories, Japan) and ethanol (99.5%) solution (1mM) for 1 h to form a self-assembled monolayer (SAM) on the surface. Then the substrate was heated for 1 h at 120°C to preserve the hydrophobic property of the substrate. In the next step, the FOPA–SAM surface was locally irradiated with focused ion beam (FIB) of Ga^+ with dosages of 4.1×10^{15} ions/cm^2 using the Versa 3D Dual Beam scanning electron microscope (FEI company) equipped with a FIB system. The chemical structure of the irradiated area by the FIB turns into hydrophilic nature, from 104° of contact angle of the pristine FOPA to 85° of the irradiated surface. Two sample substrates were prepared. Sample A is of a grid pattern of hydrophilic dots, where the diameter and interval of FIB irradiation were set at 50 and 500 nm, respectively. The full-width at half maximum of obtained dots which is a few nanometers higher than the surrounding pristine FOPA is about 110nm. Sample B has line and space pattern, whose hydrophilic lines are of 85nm width and up to 4nm height with intervals of 1.5, 2.0, 2.5, 3.0, and 3.5μm. Their AFM images are listed in Figure 5.

Nanodroplets are generated by the condensation of water vapor in the Versa 3D at environmental SEM (ESEM) mode, which enables us to observe water droplets of sub-micrometer order diameter at pressures of up to 4000 Pa. The samples are placed on a bulk copper with Peltier cooling device. At first, the pressure in the ESEM chamber is maintained at less than 100 Pa and the surface temperature is set at 0.0°C. Next, water vapor pressure in the chamber is gradually increased until condensation appeared on the surface. To avoid the evaporation of condensed droplets due to the electron beam irradiation, the voltage and current of the electron beam are set at 10 kV and <65 pA, respectively.

Droplet nucleation differs on hydrophilic and hydrophobic surfaces. This effect is explained by the difference of heterogeneous nucleation rate I on each surface [55], which is defined as:

$$I = I_0 \exp\left(-\frac{\Delta G^*}{kT}\right) \quad (1)$$

where I_0, k and T are the kinetic constant, Boltzmann constant and surface temperature, respectively. ΔG^* is the free energy of the droplet at the critical nucleation radius r^*, and it is defined as:

$$\Delta G^* = \frac{4}{3}\pi\gamma_{LV} r^{*2} f(\theta) \quad (1)$$

where γ_{LV} is the surface tension at liquid/vapor interface and $f(\theta)$ is the function of contact angle defined as follows:

$$f(\theta) = \frac{\left(2 - 3\cos\theta + \cos^3\theta\right)}{4} \quad (3)$$

Using (1)-(3), it is found that the nucleation rate of the FIB-irradiated FOPA surface is several tens of orders of magnitude higher than that of the pristine FOPA surface assuming that r^* = 2 nm. Figure 6(a) shows the condensed water droplets on the patterned surface at 560 Pa, supporting the preferential droplet condensation only on the hydrophilic FIB-irradiated dots.

During the initial stage of condensation, droplets with a diameter of about 300 nm were observed. Contact angle of these tiny droplets is about 45°, which is much lower than that of the macroscopic droplets though the three-phase contact lines are on the hydrophobic FOPA surfaces. This low contact angle is usually explained by the effect of line tension but the detailed mechanism is not clear. In addition, condensation never occurred on the hydrophobic surface close to the hydrophilic dots but some droplets condensed randomly away from the grid pattern. This phenomenon can be related with the above-described nanobubble generation near the hydrophilic domains.

By increasing the vapor pressure to 600 Pa, the condensation continues and droplets coalesced with each other into a large droplet as shown in Figure 6(b). Next, by decreasing the pressure in the ESEM chamber, the large droplet begins to evaporate and to split into many tiny ones that remained on the hydrophilic dots. Figure 6(c) shows obtained tiny droplets arranged regularly on the hydrophilic dots at 560 Pa. The enhanced variety of their size is thought to be due to the either the impurities on the FOPA surface that induces pinning of the receding motion of contact line of the droplets or the local temperature difference of the surface due to the electron beam irradiation.

The line and space pattern as listed in Figure 5(b) is also useful to generate tiny droplets by condensation. Figure 7 shows condensed droplets occurred at 0°C and 560 Pa on the hydrophilic lines of 85 nm width. Most of the condensed droplets were located on the hydrophilic lines at intervals of >1000 nm, which suggests that the observed droplets were enlarged droplets after nucleation. By using this sample substrate tilted to almost 90° relative to the horizontal surface, we captured the side view images of the submicrometer-sized droplets. The line tension τ that flattens the droplets was estimated as $\tau = -3.2 \times 10^{-9}$ N from the modified Young's equation [56] as:

$$\cos\theta = \frac{\gamma_{SV} - \gamma_{SL}}{\gamma_{LV}} - \frac{\tau}{r_c \gamma_{LV}} \qquad (4)$$

Where γ, and r_c are surface tension and contact radius of the droplet with solid surface, and subscripts S, L, and V represent the solid, liquid, and vapor phase, respectively. Obtained line tension is consistent with the reported data.[56]

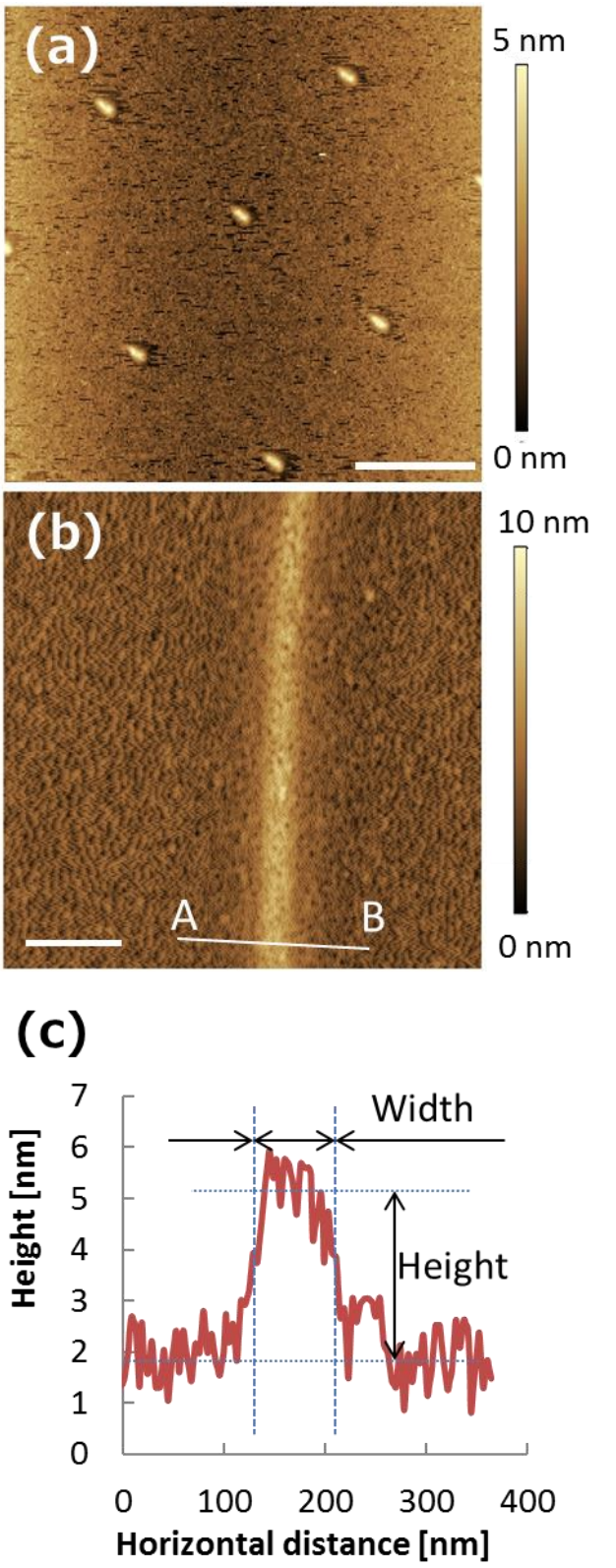

Figure 5 AFM image of FOPA surface with hydrophilic patterns fabricated by FIB irradiation; (a) dots (b) line and space. The scale bars are 1μm and 200nm, respectively. (c) Height profile of line AB in (b).

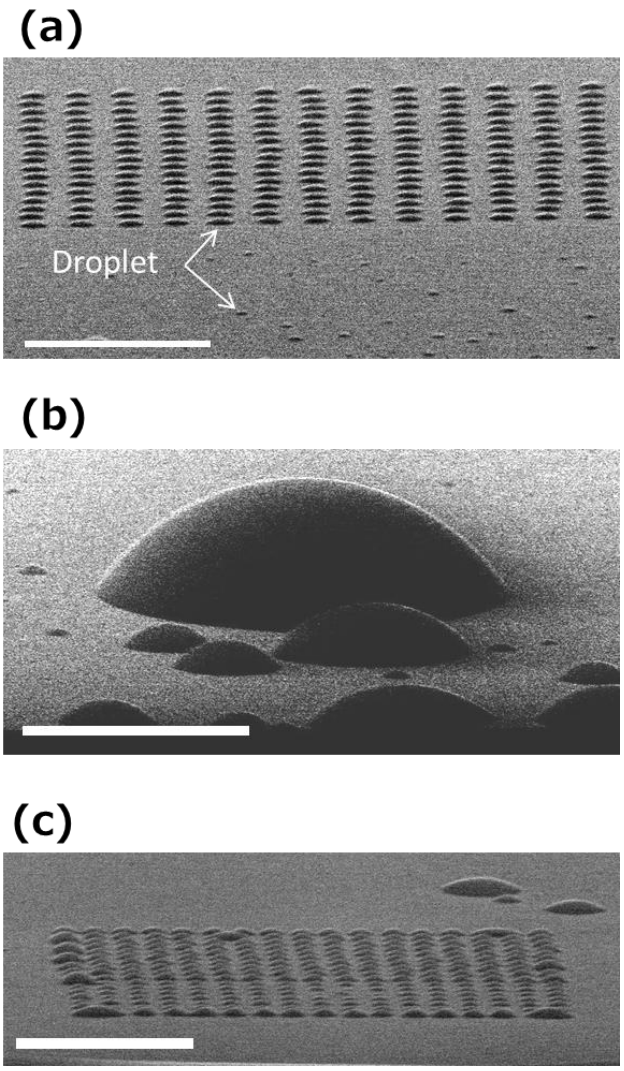

Figure 6 ESEM images of (a) initial condensed droplets, (b) enlarged water phase and (c) residual water after evaporation of (b). The scale bars are 2μm, 10μm, and 3μm, respectively.

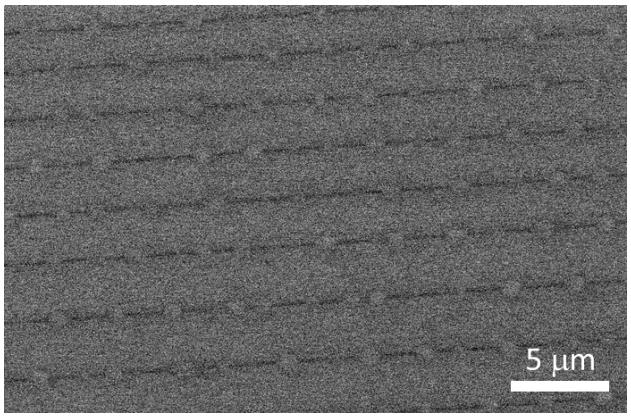

Figure 7 Condensed droplets on hydrophilic lines of 85 nm in width on a FOPA surface

CONCLUSION

A new AFM measurement mode, PF-QNM, and ESEM technique are applied for experimental studies of nanobubbles and nanodroplets, respectively. In addition to the HOPG surface that has intrinsically-combined hydrophobic/ hydrophilic surface, Teflon AF and FOPA surfaces with artificial hydrophilic domains are treated. Nanobubbles are found to generate on the hydrophobic area and to be affected by the hydrophilicity of the nearby surface. Nanodroplets are condensed preferentially on the hydrophilic surface, which is explained by the difference of heterogeneous nucleation rate. Both nanobubbles and nanodroplets are greatly flattened compared with the macroscopic ones, whose mechanism is the next research target using the contemporary experimental techniques described in this paper.

ACKNOWLEDGEMENT

This work was partially supported by CREST, JST, and JSPS KAKENHI (Grant Nos. 25420164, 26289047, 16K06126, and 16K14174). Y. Y. deeply appreciates a Grant-in-Aid for JSPS Fellows (25-4996). PF-QNM measurements were performed at the Center of Advanced Instrumental Analysis, Kyushu University.

REFERENCES

[1] Ishida, N., Inoue, T., Miyahara, M., Higashitani, K., Nano bubbles on a hydrophobic surface in water observed by tapping-mode atomic force microscopy. *Langmuir* 2000, 16, 6377–6380.

[2] Lou, S.-T., Ouyang, Z.-Q., Zhang, Y., Li, X.-J., et al., Nanobubbles on solid surface imaged by atomic force microscopy. *J. Vac. Sci. Technol. B Microelectron. Nanom. Struct.* 2000, 18, 2573.

[3] Zhang, X., Khan, A., Ducker, W.A., A Nanoscale Gas State. *Phys. Rev. Lett.* 2007, 98, 136101.

[4] Uchida, T., Oshita, S., Ohmori, M., Tsuno, T., et al., Transmission electron microscopic observations of nanobubbles and their capture of impurities in wastewater. *Nanoscale Res. Lett.* 2011, 6, 295.

[5] Seddon, J.R.T., Zandvliet, H.J.W., Lohse, D., Knudsen Gas Provides Nanobubble Stability. *Phys. Rev. Lett.* 2011, 107, 116101.

[6] Brenner, M., Lohse, D., Dynamic Equilibrium Mechanism for Surface Nanobubble Stabilization. *Phys. Rev. Lett.* 2008, 101, 1–4.

[7] Weijs, J.H., Lohse, D., Why surface nanobubbles live for hours. *Phys. Rev. Lett.* 2013, 110, 054501.

[8] Zhang, X., Chan, D.Y.C., Wang, D., Maeda, N., Stability of interfacial nanobubbles. *Langmuir* 2013, 29, 1017–1023.

[9] Liu, Y., Zhang, X., Nanobubble stability induced by contact line pinning. *J. Chem. Phys.* 2013, 138, 014706.

[10] Brotchie, A., Zhang, X.H., Response of interfacial nanobubbles to ultrasound irradiation. *Soft Matter* 2011, 7, 265.

[11] Lohse, D., Zhang, X., Pinning and gas oversaturation imply stable single surface nanobubbles. *Phys. Rev. E* 2015, 91, 031003.
[12] Lohse, D., Zhang, X., Surface nanobubbles and nanodroplets. *Rev. Mod. Phys.* 2015, 87, 981–1035.
[13] Kameda, N., Nakabayashi, S., Size-induced sign inversion of line tension in nanobubbles at a solid/liquid interface. *Chem. Phys. Lett.* 2008, 461, 122–126.
[14] Seddon, J.R.T., Bliznyuk, O., Kooij, E.S., Poelsema, B., et al., Dynamic dewetting through micropancake growth. *Langmuir* 2010, 26, 9640–4.
[15] Zhang, X., Zhang, X., Sun, J., Zhang, Z., et al., Detection of novel gaseous states at the highly oriented pyrolytic graphite-water interface. *Langmuir* 2007, 23, 1778–1783.
[16] Zhang, X., Maeda, N., Hu, J., Thermodynamic stability of interfacial gaseous states. *J. Phys. Chem. B* 2008, 112, 13671–13675.
[17] Chen, X.; Wu, J.; Ma, R.; Hua, M.; Koratkar, N.; Yao, S.; Wang, Z. Nanograssed Micropyramidal Archtectures for Continuous Dropwise Condensation. Adv. Funct. Mater. 2011, 21, 4617−4623.
[18] Miljkovic, N.; Enright, R.; Num, Y.; Lopez, K.; Dou, N.; Sack, J.; Wang, E. N. Jumping-Droplet-Enhanced Condensation on Scalable Superhydrophobic Nanostructured Surfaces. Nano Lett. 2013, 13, 179−187.
[19] Boreyko, J. B.; Chen, C. H. Self-Propelled Dropwise Condensate on Superhydrophobic Surfaces. Phys. Rev. Lett. 2009, 103, 184501.
[20] Rykaczewski, K. Microdroplet Growth Mechanism during Water Condensation on Superhydrophobic Surfaces. Langmuir 2012, 28, 7720−7729.
[21] Kim, S.; Kim, K. J. Dropwise Condensation Modeling Suitable for Superhydrophobic Surfaces. J. Heat Transfer 2011, 133, 081502.
[22] Anand, S.; Son, S. Y. Sub-Micrometer Dropwise Condensation under Superheated and Rarefied Vapor Condition. Langmuir 2010, 26, 17100−17110.
[23] Miljkovic, N.; Enright, R.; Wang, E. N. Effect of Droplet Morphology on Growth Dynamics and Heat Transfer during Condensation on Superhydrophobic Nanostructured Surfaces. ACS Nano 2012, 6, 1776−1785.
[24] Enright, R.; Miljkovic, N.; Al-Obeidi, A.; Thompson, C. V.;Wang, E. N. Condensation on Superhydrophobic Surfaces: The Role of Local Energy Barriers and Structure Length Scale. Langmuir 2012, 28, 14424−14432.
[25] Barkay, Z. Dynamic Study of Nanodroplet Nucleation and Growth on Self-Supported Nanothick Liquid Films. Langmuir 2010, 26, 18581−18584.
[26] Barkay, Z. Wettability study using transmitted electrons in environmental scanning electron microscope. Appl. Phys. Lett. 2010, 96, 183109.
[27] Rykaczewski, K.; Scott, J. H. J.; Fedorov, A. G. Electron beam heating effects during environmental scanning electron microscopy imaging of water condensation on superhydrophobic surfaces. Appl. Phys. Lett. 2011, 98, 093106.
[28] Rykaczewski, K.; Scott, J. H. J. Methodology for Imaging Nanoto-Microscale Water Condensation Dynamics on Complex Nanostructures. ACS Nano 2011, 5, 5962−5968.
[29] Varanasi, K. K.; Hsu, M.; Bhate, N.; Yang, W.; Deng, T. Spatial control in the heterogeneous nucleation of water. Appl. Phys. Lett. 2009, 95, 094101.
[30] Yao, C. W.; Garvin, T. P.; Alvarado, J. L.; Jacobi, A. M.; Jones, B. G.; Marsh, C. P. Droplet contact angle behavior on a hybrid surface with hydrophobic and hydrophilic properties. Appl. Phys. Lett. 2012, 101, 111605.
[31] Mishchenko, L.; Khan, M.; Aizenberg, J.; Hatton, B. D. Spatial Control of Condensation and Freezing on Superhydrophobic Surfaces with Hydrophilic Patches. Adv. Funct. Mater. 2013, 23, 4577−4584.
[32] Morita, M.; Koga, T.; Otsuka, H.; Takahara, A. Macroscopic-Wetting Anisotropy on the Line-Patterned Surface of Fluoroalkylsilane Monolayer. Langmuir 2005, 21, 911−918.
[33] Lee, A.; Moon, M. W.; Lim, H.; Kim, W. D.; Kim, H. Y. Water harvest via dewing. Langmuir 2012, 28, 10183−10191.
[34] Garrod, R. P.; Harris, L. G.; Schofield, W. C. E.; McGettrick, J.; Ward, L. J.; Teare, D. O. H.; Badyel, J. P. S. Mimicking a Stenocara Beetle's Back for Microcondensation Using Plasmachemical Patterned Superhydrophobic−Superhydrophilic Surfaces. Langmuir 2007, 23, 689−693.
[35] Wu, Y.; Kouno, M.; Saito, N.; Nae, F. A.; Inoue, Y.; Takai, O. Patterned hydrophobic−hydrophilic templates made from microwaveplasma enhanced chemical vapor deposited thin films. Thin Solid Films, 2007, 515, 4203−4208.
[36] Carey, V. P. Liquid−Vapor Phase-Change Phenomena: An Introduction to the Thermophysics of Vaporization and Condensation Processes in Heat Transfer Equipment; Taylor and Francis: New York, 1992.
[37] Bejan, A.; Kraus, A. D. Heat transfer handbook; Wiley: New York, 2003.
[38] Graham, C.; Griffith, P. Drop size distributions and heat transfer in dropwise condensation. Int. J. Heat Mass Transfer 1973, 16, 337−346.
[39] Zhang, X., Maeda, N., Craig, V.S.J., Physical properties of nanobubbles on hydrophobic surfaces in water and aqueous solutions. *Langmuir* 2006, 22, 5025–35.
[40] Yang, S., Dammer, S.M., Bremond, N., Zandvliet, H.J.W., et al., Characterization of nanobubbles on hydrophobic surfaces in water. *Langmuir* 2007, 23, 7072–7077.
[41] Zhang, X.H., Quinn, A., Ducker, W.A., Nanobubbles at the interface between water and a hydrophobic solid. *Langmuir* 2008, 24, 4756–64.

[42] Liu, M., Zhao, W., Wang, S., Guo, W., et al., Study on nanobubble generation: Saline solution/water exchange method. *ChemPhysChem* 2013, 14, 2589–2593.
[43] Guan, M., Guo, W., Gao, L., Tang, Y., et al., Investigation on the temperature difference method for producing nanobubbles and their physical properties. *Chemphyschem* 2012, 13, 2115–8.
[44] Guo, W., Shan, H., Guan, M., Gao, L., et al., Investigation on nanobubbles on graphite substrate produced by the water–NaCl solution replacement. *Surf. Sci.* 2012, 606, 1462–1466.
[45] Crick, C.R., Parkin, I.P., Preparation and characterisation of super-hydrophobic surfaces. *Chem. Eur. J.* 2010, 16, 3568–88.
[46] Sas, I., Gorga, R.E., Joines, J.A., Thoney, K.A., Literature review on superhydrophobic self-cleaning surfaces produced by electrospinning. *J. Polym. Sci. Part B Polym. Phys.* 2012, 50, 824–845.
[47] Weijs, J.H., Snoeijer, J., Lohse, D., Formation of surface nanobubbles and the universality of their contact angles: A molecular dynamics approach. *Phys. Rev. Lett.* 2012, 108.
[48] Seddon, J.R.T., Kooij, E.S., Poelsema, B., Zandvliet, H.J.W., Lohse, D., Surface bubble nucleation stability. *Phys. Rev. Lett.* 2011, 106, 056101.
[49] Ducker, W.A., Contact angle and stability of interfacial nanobubbles. *Langmuir* 2009, 25, 8907–10.
[50] Yang, S., Kooij, E.S., Poelsema, B., Lohse, D., Zandvliet, H.J.W., Correlation between geometry and nanobubble distribution on HOPG surface. *Europhys. Lett.* 2008, 81, 64006.
[51] Craig, V.S.J., Very small bubbles at surfaces—the nanobubble puzzle. *Soft Matter* 2011, 7, 40.
[52] Walczyk, W., Schönherr, H., Closer look at the effect of AFM imaging conditions on the apparent dimensions of surface nanobubbles. *Langmuir* 2013, 29, 620–32.
[53] Walczyk, W., Schön, P.M., Schönherr, H., The effect of PeakForce tapping mode AFM imaging on the apparent shape of surface nanobubbles. *J. Phys. Condens. Matter* 2013, 25, 184005.
[54] Zhao, B., Song, Y., Wang, S., Dai, B., et al., Mechanical mapping of nanobubbles by PeakForce atomic force microscopy. *Soft Matter* 2013, 9, 8837.
[55] Sigsbee, R. A., in Nucleation, edited by A. C. Zettelmoyer, Marcel Dekker, New York, 1969.
[56] Drelich, J. The significance and magnitude of the line tension in three-phase (solid−liquid−fluid) systems. Colloids Surf., A 1996, 116, 43−54.